STRUCTURAL BIOLOGY COMMUNICATIONS

ISSN 2053-230X

Production, crystallization and neutron diffraction of fully deuterated human myelin peripheral membrane protein P2

Saara Laulumaa,[a,b] Matthew P. Blakeley,[c] Arne Raasakka,[a,d] Martine Moulin,[e] Michael Härtlein[e] and Petri Kursula[a,d]*

[a]Faculty of Biochemistry and Molecular Medicine and Biocenter Oulu, University of Oulu, PO Box 5400, 90014 Oulu, Finland, [b]European Spallation Source, Lund, Sweden, [c]Large-Scale Structures Group, Institut Laue–Langevin, 71 Avenue des Martyrs, 38000 Grenoble, France, [d]Department of Biomedicine, University of Bergen, 5009 Bergen, Norway, and [e]Life Sciences Group, Institut Laue–Langevin, 71 Avenue des Martyrs, 38000 Grenoble, France. *Correspondence e-mail: petri.kursula@uib.no

Received 1 September 2015
Accepted 24 September 2015

Edited by W. N. Hunter, University of Dundee, Scotland

Keywords: perdeuteration; neutron diffraction; fatty acid-binding protein; myelin; peripheral membrane protein.

The molecular details of the formation of the myelin sheath, a multilayered membrane in the nervous system, are to a large extent unknown. P2 is a peripheral membrane protein from peripheral nervous system myelin, which is believed to play a role in this process. X-ray crystallographic studies and complementary experiments have provided information on the structure–function relationships in P2. In this study, a fully deuterated sample of human P2 was produced. Crystals that were large enough for neutron diffraction were grown by a ten-month procedure of feeding, and neutron diffraction data were collected to a resolution of 2.4 Å from a crystal of 0.09 mm^3 in volume. The neutron crystal structure will allow the positions of H atoms in P2 and its fatty-acid ligand to be visualized, as well as shedding light on the fine details of the hydrogen-bonding networks within the P2 ligand-binding cavity.

1. Introduction

Myelin is a multilayered proteolipid membrane structure formed by dozens of tightly packed bilayers of a glial cell plasma membrane. Myelinating glial cells include Schwann cells in peripheral nerves and oligodendrocytes in the central nervous system. A number of specific myelin proteins, which are largely specific to vertebrates, are believed to be crucial for the formation and maintenance of a healthy myelin sheath (Gould *et al.*, 2008; Han *et al.*, 2013). Myelin-related neurodegenerative diseases may be caused by inherited mutations in myelin protein genes as well as by an autoimmune attack against myelin proteins (Trapp *et al.*, 1996).

One of the myelin-specific proteins in peripheral nerves is P2, a peripheral membrane protein belonging to the fatty acid-binding protein (FABP) family (Jones *et al.*, 1988; Hunter *et al.*, 2005; Majava *et al.*, 2010; Storch & Thumser, 2010). P2 binds to lipid-membrane surfaces, and it is also able to spontaneously stack lipid bilayers into multilayers (Sedzik *et al.*, 1985; Suresh *et al.*, 2010; Ruskamo *et al.*, 2014; Laulumaa, Nieminen *et al.*, 2015). We have previously refined the X-ray crystal structure of human P2 to 0.93 Å resolution, enabling the visualization of accurate structural details, including certain protonation states and hydrogen-bonding networks (Ruskamo *et al.*, 2014). Conformational changes and protein dynamics of P2 are likely to play major roles in protein–membrane interactions and lipid ligand binding, as suggested by structural studies, neutron scattering experiments and

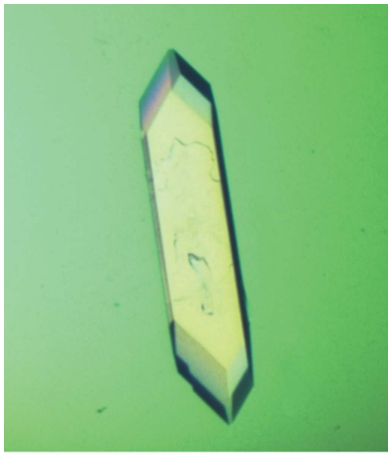

Table 1
Production of perdeuterated human P2.

Source organism	*Homo sapiens*
Expression vector	pETNKI-his3C-LIC-Kan
Expression host	*E. coli* Rosetta (DE3)
Complete amino-acid sequence	GMSNKFLGTWKLVSSENFDDYMKALGVGLATRKLGNLA-KPTVIISKKGDIITIRTESTFKNTEISFKLGQEFEE-TTADNRKTKSIVTLQRGSLNQVQRWDGKETTIKRKL-VNGKMVAECKMKGVVCTRIYEKV

computer simulations (Ruskamo *et al.*, 2014; Laulumaa, Nieminen *et al.*, 2015; Laulumaa, Kursula *et al.*, 2015).

P2 deficiency does not appear to cause abnormalities in myelin ultrastructure in mouse peripheral nerves (Zenker *et al.*, 2014). Young P2-deficient mice, however, show mildly decreased motor neuron conduction velocity and aberrant lipid profiles during the period of most active myelination (Zenker *et al.*, 2014). Very recently, a point mutation in human P2 has been linked to inherited neuropathies (Gonzaga-Jauregui *et al.*, 2015). P2 has also been considered to be a potential autoantigen in Guillain–Barré syndrome, which is a human autoimmune peripheral neuropathy (Offenhäusser *et al.*, 2002; Csurhes *et al.*, 2005; Hughes & Cornblath, 2005; Makowska *et al.*, 2008). The detailed P2-related molecular mechanisms behind the links to these diseases are currently unknown.

In this paper, we present the production and crystallization of fully deuterated (perdeuterated) recombinant human P2 protein. The neutron diffraction data will allow the visualization of H atoms (as deuterium) in this abundant peripheral membrane protein.

2. Materials and methods

2.1. Recombinant protein production and characterization

The cDNA of human myelin protein P2 with an N-terminal *Tobacco etch virus* (TEV) protease-cleavable 6×His tag (Majava *et al.*, 2010) was cloned into the pETNKI-his3C-LIC-Kan vector (Busso *et al.*, 2011) using the SLIC cloning protocol (Li & Elledge, 2012). Protein expression was performed at the deuteration laboratory at the Institut Laue–Langevin (ILL), Grenoble, France. Perdeuterated P2 was expressed in *Escherichia coli* Rosetta (DE3) cells in fully deuterated minimal medium (Artero *et al.*, 2005), using glycerol-d_8 as the carbon source (Table 1). *E. coli* cells were adapted to deuterated conditions, from fully hydrogenated to fully deuterated medium, in six 1:10 inoculation steps. Perdeuterated P2 protein was then expressed in a 1 l culture at 293 K in a Labfors fermenter (Infors).

Protein purification was based on the previously described protocol for P2 (Majava *et al.*, 2010; Lehtimäki *et al.*, 2012). 5 g of harvested *E. coli* pellet mass was suspended in 50 ml lysis buffer (50 m*M* sodium phosphate, 300 m*M* NaCl, 10 m*M* imidazole pH 8.0) and lysed by six cycles of sonication for 30 s using a Bandelin Sonopuls sonicator. Cell debris was removed by centrifugation at 11 000*g* and 277 K for 40 min. Cell lysis was repeated twice for the pellet in order to increase the yield of pure protein.

The supernatant containing soluble P2 was filtered and loaded onto a Ni–NTA matrix (Qiagen) in a gravity-flow column. The matrix was washed with lysis buffer, and bound proteins were eluted with elution buffer (50 m*M* sodium phosphate, 300 m*M* NaCl, 400 m*M* imidazole pH 8.0). His tags were cleaved in an overnight TEV protease digestion, while dialyzing against imidazole-free buffer (50 m*M* sodium phosphate, 300 m*M* NaCl pH 8.0) at room temperature. The His tags, uncleaved protein and His-tagged TEV were removed by running the mixture through the Ni–NTA matrix. Cleaved P2 protein in the flowthrough was further purified by size-exclusion chromatography. The concentrated protein sample was loaded onto a Superdex 75 16/60 column (GE Healthcare) and eluted with a buffer consisting of 150 m*M* NaCl, 10% glycerol, 20 m*M* HEPES pH 7.5 at a flow rate of 1 ml min^{-1}. The total yield was 0.5 mg pure perdeuterated P2 protein from 1 g *E. coli* paste.

The degree of perdeuteration of P2 was determined by mass spectrometry. Samples of perdeuterated and hydrogenated P2 were mixed with an excess of 0.1% trifluoroacetic acid in either D_2O or H_2O, respectively, and mass spectra were acquired using a Waters Acquity Synapt G2 time-of-flight mass analyzer with a Z-spray electrospray ionization source. The obtained masses were compared with theoretical values. The total amount of hydrogen in P2 was calculated using *ProtParam* (Gasteiger *et al.*, 2005).

2.2. Crystallization

For crystallization, the deuterated protein was exchanged into deuterated buffer (150 m*M* NaCl, 10% glycerol, 20 m*M* HEPES pD 7.5) in 99.90% D_2O (Euriso-top) by concentrating the protein solution using centrifugal ultrafiltration and diluting it back into deuterated buffer repeatedly. pD was defined as the measured pH + 0.4 units.

Protein crystals were grown in hanging drops using 24-well crystallization plates and glass cover slides (Hampton Research). Crystal growth was optimal at 281 K when 28% PEG 6000, 0.1 *M* citrate (pD 4.75) was used as the reservoir solution. The protein concentration was 2.5 mg ml^{-1}, with a 1:1 protein buffer:reservoir solution volume ratio in the drops. Typically, long, rod-shaped crystals formed within a week.

Firstly, several crystals of 0.1 mm in length were grown in 3 µl hanging drops. These seed crystals were then transferred to fresh 3 µl drops, with one crystal per drop, to maximize the growth of large single crystals. Crystals were fed with 3 µl of fresh protein and reservoir solution in a 1:1 ratio every 2–3 weeks. Once the drops were around 20 µl in size, 3 µl of drop solution was removed before the addition of fresh protein. In addition to keeping the drop volume at reasonable levels, the latter was performed to avoid concentration gradients in the drop and crystal nucleation while feeding.

During ten months of feeding, crystals grew to ∼0.3 mm^3 in volume. Three of them were mounted in 2 mm quartz capillaries and tested using the quasi-Laue cold neutron

Table 2
Mass-spectrometric analysis of recombinant P2 deuteration.

	Molecular weight† (Da)			No. of hydrogens/deuteriums		
Sample	Theoretical	Determined	Difference	Theoretical‡	Measured	Deuteration (%)
Hydrogenated P2, H_2O	14966.4	14962.5	−3.9	1095	1091	0
Perdeuterated P2, D_2O	16068.0	16030.5	−37.5	1095	1058	96.6

† The theoretical and determined masses correspond to those for the reduced protein. ‡ Determined using *ProtParam*.

diffractometer LADI-III (Blakeley *et al.*, 2010) at ILL. The diffraction spots from the largest two crystals were streaked, but the smallest 0.09 mm^3 crystal diffracted with small, distinct spots to a reasonable resolution and was thus chosen for data collection.

2.3. Neutron diffraction data collection and processing

Neutron diffraction data were collected from a perdeuterated crystal of P2 myelin protein (volume of ∼0.09 mm^3) at 292 K using LADI-III at the ILL. In 2012, LADI-III was relocated to a new guide, H143, closer to the ILL high-flux reactor. This new end position provides an improved bandpass profile (owing to the lack of instruments upstream) and a fourfold increase in flux at the sample position compared with the previous H142 position, allowing smaller crystal volumes to be used for data collection (Blakeley *et al.*, 2015). A Ni/Ti multilayer bandpass filter was used to select a restricted neutron wavelength range ($\delta\lambda/\lambda \simeq 25\%$) centred at 3.6 Å and extending from 3.0 to 3.9 Å. As is typical for a Laue diffraction experiment, the crystal was held stationary at a different φ setting (*i.e.* the vertical rotation axis of the cylindrical neutron-sensitive image-plate detector) for each exposure. Initially, eight contiguous images ($\Delta\varphi = 7^\circ$) were collected and the orientation of the crystal was then altered and a second series of 11 contiguous images were collected before the reactor cycle ended. In order to improve the completeness of the neutron data set, further data collection was scheduled for the following reactor cycle; however, by this time the crystal had deteriorated such that further data collection was not possible. Neutron diffraction data to 2.4 Å resolution were indexed and integrated using the Daresbury Laboratory software *LAUEGEN* (Helliwell *et al.*, 1989; Campbell, 1995) modified for the cylindrical geometry of the detector (Campbell *et al.*, 1998). The *LSCALE* program (Arzt *et al.*, 1999) was used to derive the wavelength-normalization curve using the intensities of symmetry-equivalent reflections measured at different wavelengths. No provision was needed for radiation damage, and no explicit absorption corrections were applied. Data were merged using *SCALA* and converted to structure factors using *TRUNCATE* from the *CCP*4 suite (Winn *et al.*, 2011).

3. Results and discussion

Milligram amounts of recombinant perdeuterated human P2 were produced using standardized protocols (Majava *et al.*, 2010; Lehtimäki *et al.*, 2012) in order to obtain labelled material for neutron scattering and diffraction experiments (Fig. 1). The total protein deuteration level, as determined by mass spectrometry, was 96.6% (Table 2). Thus, the produced recombinant human P2 could be considered to be perdeuterated.

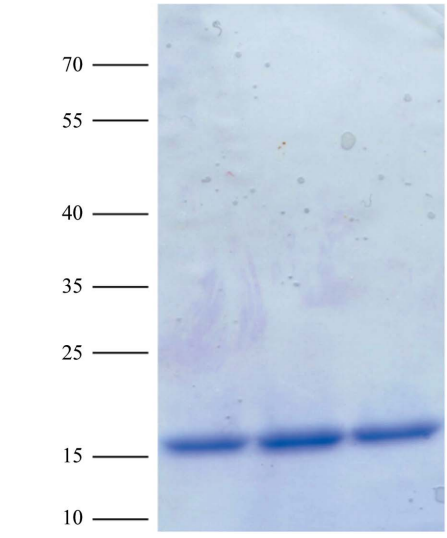

(*a*)

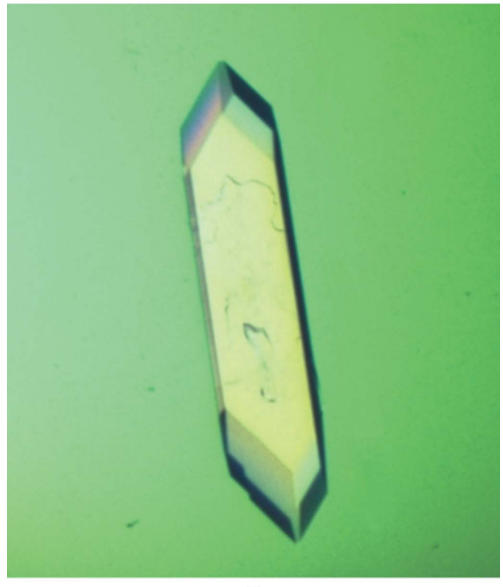

(*b*)

Figure 1
Purification and crystallization of deuterated human P2. (*a*) SDS–PAGE analysis of three purified fractions of perdeuterated P2 (16 kDa) from size-exclusion chromatography. (*b*) A typical crystal of perdeuterated human P2 during feeding. The maximum dimension of the crystal is ∼1 mm.

Table 3
Data collection and processing.

Values in parentheses are for the outer shell.

Diffraction source	LADI-III, ILL
Wavelength range (Å)	3.0–3.9
Temperature (K)	292
No. of images	19
Angle between images (°)	7
Average exposure time (min)	1412
Space group	$P4_12_12$
a, b, c (Å)	57.95, 57.95, 100.79
α, β, γ (°)	90, 90, 90
Resolution range (Å)	40–2.40 (2.53–2.40)
Total No. of reflections	17607 (810)
No. of unique reflections	4232 (363)
Completeness (%)	60.1 (36.9)
Multiplicity	4.2 (2.2)
$\langle I/\sigma(I)\rangle$	6.1 (2.8)
$R_{\rm merge}$	0.189 (0.304)
$R_{\rm p.i.m.}$	0.081 (0.207)

Crystals of perdeuterated P2 were grown over a period of several months with repeating cycles of feeding with fresh protein (Fig. 1). Several crystals with maximum dimensions of >1 mm were obtained using this procedure, and a neutron diffraction data set was collected from a single crystal of <0.1 mm^3 (Fig. 2, Table 3). Of the three tested crystals, the smallest one provided neat, indexable data, while the larger crystals were more poorly ordered. The space group was identical to that observed for the hydrogenated protein, and the unit-cell parameters were very close to those in our earlier atomic resolution structure of human P2. Unfortunately, time constraints prevented the collection of a more complete data set, but considering the full deuteration of the sample and solvent and the availability of joint X-ray/neutron refinement, the data will be suitable for structural analyses. Rather incomplete neutron data have also been used for structural studies previously (Afonine *et al.*, 2010).

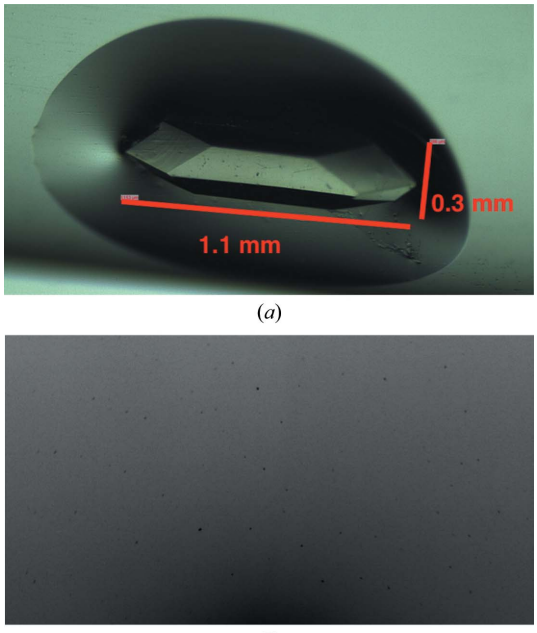

(*a*)

(*b*)

Figure 2
Neutron diffraction data collection from a crystal of human P2. (*a*) The crystal used for data collection, mounted in a quartz capillary. The dimensions of the crystal are shown. (*b*) Neutron diffraction image with diffraction to 2.4 Å resolution.

The processed data extended to a resolution of 2.4 Å. This resolution should allow the visualization of a large number of ordered H atoms (as deuterium) in the crystal structure, once joint refinement with a corresponding X-ray diffraction data set can be carried out. A number of other properties, such as amino-acid protonation states, orientation of water molecules and protein–ligand interactions, can most likely be deduced from joint X-ray/neutron refinement (Langan & Chen, 2013; Oksanen *et al.*, 2014). Coupled with our previous atomic resolution X-ray crystal structure of human P2 (Ruskamo *et al.*, 2014), as well as our studies on P2 dynamics (Laulumaa, Nieminen *et al.*, 2015), these complementary data will allow a much more detailed picture of P2 and its ligand-recognition determinants to be obtained. Our high-resolution X-ray crystal structure at 100 K already allowed much of the organization of the internal hydrogen-bonding networks within the P2 fatty acid-binding cavity to be deduced (Ruskamo *et al.*, 2014). However, the hydrogen substructure of a protein is often not clear even at very high X-ray resolutions, especially at functional or flexible sites. It is also likely that there are differences in the hydrogen-bonding networks between the high-resolution X-ray crystal structure at 100 K and the lower resolution neutron crystal structure in D_2O at ambient temperature.

To conclude, we have taken the first steps towards obtaining neutron crystallographic structural data on human P2, an abundant peripheral membrane protein of myelinating Schwann cells. The successful production and crystallization of perdeuterated P2, together with neutron diffraction data collection, will allow a more detailed view of the protonation states and hydrogen-bonding networks in this membrane-associating molecule to be obtained. Details of protein–fatty acid interaction determinants should also become visible, especially for the hydrocarbon tail of the bound ligand. From another point of view, the neutron data sample a large crystal volume, and considering that these experiments were carried out in ambient temperature as opposed to 100 K, we expect to also obtain an idea of protein dynamics using these data. In addition to the neutron diffraction data presented here, a corresponding X-ray diffraction data set has recently been collected under ambient conditions, and joint refinement is under way. It is most probable that the results from neutron refinement of P2 will also be applicable to structure–function studies on other members of the FABP family.

Acknowledgements

This study has been supported by grants from the Academy of Finland, the Emil Aaltonen Foundation (Finland) and the Sigrid Jusélius Foundation (Finland). We wish to thank the ILL for beamtime and the Biocenter Oulu Proteomics Core Facility for instrumentation.

References

Afonine, P. V., Mustyakimov, M., Grosse-Kunstleve, R. W., Moriarty, N. W., Langan, P. & Adams, P. D. (2010). *Acta Cryst.* D**66**, 1153–1163.

Artero, J.-B., Härtlein, M., McSweeney, S. & Timmins, P. (2005). *Acta Cryst.* D**61**, 1541–1549.

Arzt, S., Campbell, J. W., Harding, M. M., Hao, Q. & Helliwell, J. R. (1999). *J. Appl. Cryst.* **32**, 554–562.

Blakeley, M. P., Hasnain, S. S. & Antonyuk, S. V. (2015). *IUCrJ*, **2**, 464–474.

Blakeley, M. P., Teixeira, S. C. M., Petit-Haertlein, I., Hazemann, I., Mitschler, A., Haertlein, M., Howard, E. & Podjarny, A. D. (2010). *Acta Cryst.* D**66**, 1198–1205.

Busso, D. *et al.* (2011). *J. Struct. Biol.* **175**, 159–170.

Campbell, J. W. (1995). *J. Appl. Cryst.* **28**, 228–236.

Campbell, J. W., Hao, Q., Harding, M. M., Nguti, N. D. & Wilkinson, C. (1998). *J. Appl. Cryst.* **31**, 496–502.

Csurhes, P. A., Sullivan, A. A., Green, K., Pender, M. P. & McCombe, P. A. (2005). *J. Neurol. Neurosurg. Psychiatry*, **76**, 1431–1439.

Gasteiger, E., Hoogland, C., Gattiker, A., Duvaud, S., Wilkins, M. R., Appel, R. D. & Bairoch, A. (2005). *The Proteomics Protocols Handbook*, edited by J. M. Walker, pp. 571–607. Totowa: Humana Press.

Gonzaga-Jauregui, C. *et al.* (2015). *Cell Rep.* **12**, 1169–1183.

Gould, R. M., Oakley, T., Goldstone, J. V., Dugas, J. C., Brady, S. T. & Gow, A. (2008). *Neuron Glia Biol.* **4**, 137–152.

Han, H., Myllykoski, M., Ruskamo, S., Wang, C. & Kursula, P. (2013). *Biofactors*, **39**, 233–241.

Helliwell, J. R., Habash, J., Cruickshank, D. W. J., Harding, M. M., Greenhough, T. J., Campbell, J. W., Clifton, I. J., Elder, M., Machin, P. A., Papiz, M. Z. & Zurek, S. (1989). *J. Appl. Cryst.* **22**, 483–497.

Hughes, R. A. & Cornblath, D. R. (2005). *Lancet*, **366**, 1653–1666.

Hunter, D. J. B., Macmaster, R., Roszak, A. W., Riboldi-Tunnicliffe, A., Griffiths, I. R. & Freer, A. A. (2005). *Acta Cryst.* D**61**, 1067–1071.

Jones, T. A., Bergfors, T., Sedzik, J. & Unge, T. (1988). *EMBO J.* **7**, 1597–1604.

Langan, P. & Chen, J. C.-H. (2013). *Phys. Chem. Chem. Phys.* **15**, 13705.

Laulumaa, S., Kursula, P. & Natali, F. (2015). *EPJ Web Conf.* **83**, 02010.

Laulumaa, S., Nieminen, T., Lehtimaki, M., Aggarwal, S., Simons, M., Koza, M. M., Vattulainen, I., Kursula, P. & Natali, F. (2015). *PLoS One*, **10**, e0128954.

Lehtimäki, M., Laulumaa, S., Ruskamo, S. & Kursula, P. (2012). *Acta Cryst.* F**68**, 1359–1362.

Li, M. Z. & Elledge, S. J. (2012). *Methods Mol. Biol.* **852**, 51–59.

Majava, V., Polverini, E., Mazzini, A., Nanekar, R., Knoll, W., Peters, J., Natali, F., Baumgärtel, P., Kursula, I. & Kursula, P. (2010). *PLoS One*, **5**, e10300.

Makowska, A., Pritchard, J., Sanvito, L., Gregson, N., Peakman, M., Hayday, A. & Hughes, R. (2008). *J. Neurol. Neurosurg. Psychiatry*, **79**, 664–671.

Offenhäusser, M., Herr, A. S., Hartkamp, J., Wauben, M., Magnus, T., Grauer, O., Seubert, S., Weishaupt, A., Toyka, K. V., Gold, R. & Troppmair, J. (2002). *J. Neuroimmunol.* **129**, 97–105.

Oksanen, E., Blakeley, M. P., El-Hajji, M., Ryde, U. & Budayova-Spano, M. (2014). *PLoS One*, **9**, e86651.

Ruskamo, S., Yadav, R. P., Sharma, S., Lehtimäki, M., Laulumaa, S., Aggarwal, S., Simons, M., Bürck, J., Ulrich, A. S., Juffer, A. H., Kursula, I. & Kursula, P. (2014). *Acta Cryst.* D**70**, 165–176.

Sedzik, J., Blaurock, A. E. & Hoechli, M. (1985). *J. Neurochem.* **45**, 844–852.

Storch, J. & Thumser, A. E. (2010). *J. Biol. Chem.* **285**, 32679–32683.

Suresh, S., Wang, C., Nanekar, R., Kursula, P. & Edwardson, J. M. (2010). *Biochemistry*, **49**, 3456–3463.

Trapp, B. D., Haney, C. & Yin, X. (1996). *Rev. Neurol.* **152**, 314–319.

Winn, M. D. *et al.* (2011). *Acta Cryst.* D**67**, 235–242.

Zenker, J., Stettner, M., Ruskamo, S., Domènech-Estévez, E., Baloui, H., Médard, J.-J., Verheijen, M. H. G., Brouwers, J. F., Kursula, P., Kieseier, B. C. & Chrast, R. (2014). *Glia*, **62**, 1502–1512.